

Article

Biocompatibility and Antibiofilm Properties of Samarium Doped Hydroxyapatite Coatings: An *In Vitro* Study

Ionela Cristina Nica ^{1,2} , Marcela Popa ^{2,3} , Luminita Marutescu ^{2,3}, Anca Dinischiotu ^{1,*},
Simona Liliana Iconaru ⁴, Steluta Carmen Ciobanu ⁴ and Daniela Predoi ⁴

¹ Department of Biochemistry and Molecular Biology, Faculty of Biology, University of Bucharest, 91-95 Splaiul Independentei, 050095 Bucharest, Romania; cristina.nica@drd.unibuc.ro

² Research Institute of the University of Bucharest–ICUB, University of Bucharest, 050657 Bucharest, Romania; bmarcelica@yahoo.com (M.P.); lumi.marutescu@gmail.com (L.M.)

³ Microbiology Department, Faculty of Biology, University of Bucharest, 1-3 Portocalelor Lane, 077206 Bucharest, Romania

⁴ National Institute of Materials Physics, Atomistilor Street No. 405A, 077125 Magurele, Romania; simona.iconaru@infim.ro (S.L.I.); carmen.ciobanu@infim.ro (S.C.C.); dpredoi@infim.ro (D.P.)

* Correspondence: anca.dinischiotu@bio.unibuc.ro; Tel.: +40-21-318-1575

Abstract: The implant-related infection as a consequence of bacterial adherence and biofilm formation remains one of the main causes of implant failure. Grace to recent advances in materials science, their great mechanical properties and their biocompatibility (both *in vitro* and *in vivo*), antibacterial coatings have gradually become a primary component of the global strategy for preventing microbial colonization. In the present work, novel antibacterial coatings containing hydroxyapatite nanoparticles doped with two different concentrations of samarium (5SmHAp and 10SmHAp) were obtained on Si substrates using the dip coating method. The morphology and physicochemical properties of these modified surfaces were characterized by X-ray diffraction (XRD), scanning electron microscopy (SEM) and Fourier transform infrared spectroscopy (FTIR). In addition, their antimicrobial effects and biocompatibility were assessed. The results showed a continuous and homogeneous layer, uniformly deposited, with no cracks or impurities. 5SmHAp and 10SmHAp surfaces exhibited significant antibiofilm activity and good biocompatibility without inducing cytotoxic effects in human gingival fibroblasts. All these findings indicate that samarium doped hydroxyapatite coatings could be great candidates for the development of new antimicrobial strategies.

Keywords: dip coating technique; samarium; hydroxyapatite; antibacterial coatings; biocompatibility



Citation: Nica, I.C.; Popa, M.; Marutescu, L.; Dinischiotu, A.; Iconaru, S.L.; Ciobanu, S.C.; Predoi, D. Biocompatibility and Antibiofilm Properties of Samarium Doped Hydroxyapatite Coatings: An *In Vitro* Study. *Coatings* **2021**, *11*, 1185. <https://doi.org/10.3390/coatings11101185>

Academic Editor: Maria Cristina Tanzi

Received: 31 August 2021

Accepted: 26 September 2021

Published: 29 September 2021

Publisher's Note: MDPI stays neutral with regard to jurisdictional claims in published maps and institutional affiliations.



Copyright: © 2021 by the authors. Licensee MDPI, Basel, Switzerland. This article is an open access article distributed under the terms and conditions of the Creative Commons Attribution (CC BY) license (<https://creativecommons.org/licenses/by/4.0/>).

1. Introduction

Tens of millions of metal implants and medical alloys are used each year for orthopedic and dental purposes in order to assure tissue support and to promote osseointegration with the surrounding bone [1]. The success rate of these implantable devices depends mainly on their biocompatibility and the capacity of their surface to host different cells responsible for the healing and regeneration processes [2]. In this regard, hydroxyapatite (HAp) based coatings have been widely used in biomedicine for the last 5 decades due to its excellent biocompatibility, bioactivity and osteoconductive properties [3]. One of the main reasons why this bioceramic material is so used is its chemical similarity with the inorganic component of human bone structures [4]. In addition, HAp coatings have the ability to enhance the implant-tissue interactions, shortening the healing process of metal-containing implants, and act as an anti-corrosive barrier against body fluids, while minimizing the dissolution rate and risk of metallic ions leakage, without altering the material's properties [5].

Despite all the advances in the field of biomaterials, the introduction of a foreign material in the body is most often associated with bacterial colonization and implant-related

infections (peri-implantitis), leading to severe complications and eventual failure [6]. Certain gram-positive and gram-negative bacterial strains are capable of forming a protective biofilm layer on medical devices, protecting them from exposure to host immune defense and antibiotics [7,8].

Since the metals and alloys used in the manufacture of implants do not have intrinsic antiseptic qualities, there is an urgent need for the development of modified surfaces with increased antimicrobial and antibiofilm potential; but these strategies should not alter the physicochemical properties of the original surfaces in order to maintain biocompatibility with the surrounding tissues [9]. Several approaches have been conducted to transform biomedical devices into antibacterial surfaces, but those containing permanently bound agents are the only ones that have succeeded in creating a long-term antimicrobial environment [10]. These techniques include surface-bound antibiotics, silver-implanted surfaces, polymer-functionalized surfaces and UV-activated surfaces [11].

The lanthanides also occupy an important niche in this field. Due to their unique functionalities, these rare-earth elements received more attention in the last decades. Trivalent lanthanide ions (Ln^{3+}) exhibit excellent electromagnetic and luminescent properties because of the presence of unpaired electrons in their 4f orbitals [12]. Thus, they can be successfully used as fluorescent dyes and contrast agents in bioimaging, biosensing, controlled drug delivery, cancer therapy, and cellular activity control and monitoring [13,14]. Several lanthanides, including cerium, are well-known for their anticoagulant properties and have been employed as antithrombic drugs [15–17]. The antibacterial effects of Ln^{3+} were first observed at the end of the 19th century when several cerium(III) salts (acetate, chloride, stearate, and nitrate) were reported to have broad-spectrum antibacterial activity and the oxidizing properties of cerium(IV) led to the use of cerium(IV) sulfate as an antiseptic powder [18]. Moreover, recent studies showed that different lanthanide complexes exhibited better antimicrobial activities compared to the standard antibiotics [19]; the antimicrobial properties possessed by the lanthanides are considered to be a complex combination of several factors such as: the nature of the metal ion, interaction of metal ions with cellular components, chelation, coordinating sites, geometry of the complex, concentration, hydrophilicity, lipophilicity, steric and pharmacokinetic factors as well as other environmental factors [20].

Considering that lanthanides may represent a possible alternative to the currently used antimicrobial agents and a suitable strategy for prevention of postoperative infections after implant surgery, in the present work novel samarium (Sm^{3+}) doped HAp coatings were obtained and characterized. Samarium was selected for several reasons: (i) Sm^{3+} has been already used in clinic to target the bone tissue, exhibiting low toxicity and an adequate safety profile [21], (ii) it appears not to affect the behavior of osteoblasts [22], and (iii) our previous studies reported superior antimicrobial properties of Sm^{3+} containing materials [23,24]. But to the best of our knowledge, the samarium doped hydroxyapatite coatings with antimicrobial properties developed by dip coating technique as well as their influence on gingival fibroblasts have not been addressed so far. Therefore, samarium oxide doped HAp coatings were prepared with two lanthanide concentrations, and characterized for the physicochemical profile as well as for their biological response and antibacterial and antifungal properties.

2. Materials and Methods

2.1. Materials

In order to obtain samarium doped hydroxyapatite ($\text{Ca}_{10-x}\text{Sm}_x(\text{PO}_4)_6(\text{OH})_2$, $x_{\text{Sm}} = 0.05$ and 0.1) calcium nitrate tetrahydrate, $\text{Ca}(\text{NO}_3)_2 \cdot 4\text{H}_2\text{O}$ ($\geq 99.0\%$, Sigma Aldrich, St. Louis, MO, USA), samarium nitrate hexahydrate, $\text{Sm}(\text{NO}_3)_3 \cdot 6\text{H}_2\text{O}$ (99.97%, Alpha Aesar, Kandel, Germany), ammonium hydrogen phosphate, $(\text{NH}_4)_2\text{HPO}_4$ ($\geq 99.0\%$, Sigma Aldrich, St. Louis, MO, USA), absolute ethanol, $\text{C}_2\text{H}_5\text{OH}$ ($\geq 99.8\%$, Sigma Aldrich, St. Louis, MO, USA) and double distilled water were used as precursors.

2.2. Samarium Doped Hydroxyapatite (SmHAp)

An adapted method was used in order to obtain samarium doped hydroxyapatite nanoparticles ($\text{Ca}_{10-x}\text{Sm}_x(\text{PO}_4)_6(\text{OH})_2$, $x_{\text{Sm}} = 0.05$ and 0.1). The value of $(\text{Ca} + \text{Sm})/P$ was 1.67. Therefore, the samarium doped hydroxyapatite was synthesized as previously described by Ciobanu et al. [25]. Therefore, two solutions were firstly obtained as follows: calcium nitrate tetrahydrate was dissolved in absolute ethanol (100 mL) thus, obtaining the S1 solution; ammonium hydrogen phosphate was dissolved in 25 mL of deionized water obtaining S2 solution. The obtained solutions (S1 and S2) were mixed and stirred together in ambient condition for 1 h. Secondly, samarium nitrate hexahydrate was dissolved in 25 mL of deionized water, then dropwise in the first mixture at $100\text{ }^\circ\text{C}$ and stirred for 2 h. After 2 h, the solution was centrifugated and dispersed in absolute ethanol [25]. The obtained suspensions were used to prepare the coatings.

2.3. Preparation of SmHAp Coatings

The 5SmHAp ($\text{Ca}_{10-x}\text{Sm}_x(\text{PO}_4)_6(\text{OH})_2$, $x_{\text{Sm}} = 0.05$) and 10SmHAp ($\text{Ca}_{10-x}\text{Sm}_x(\text{PO}_4)_6(\text{OH})_2$, $x_{\text{Sm}} = 0.1$) coatings have been deposited on the Si wafer using the dip coating method in agreement with previous studies [25]. The Si substrate was cleaned with absolute ethanol before coatings deposition. Then, the Si substrate was immersed in the previously obtained solutions in order to obtain the 5SmHAp and 10SmHAp thin films. After the deposition of 5SmHAp and 10SmHAp coatings they were dried $100\text{ }^\circ\text{C}$ for 4 h and after treated at $500\text{ }^\circ\text{C}$ for 2 h.

2.4. Physicochemical Characterization Methods

The structural investigation was conducted on the obtained SmHAp coatings using a D8 Advance diffractometer (Bruker, Karlsruhe, Germany) equipped with a nickel filtered $\text{Cu K}\alpha$ ($\lambda = 1.5418\text{ \AA}$) radiation and a high efficiency one-dimensional detector (Lynx Eye type) operated in integration mode. The diffractograms were acquired in the 2θ range 20° – 80° .

Scanning electron microscopy (SEM) was used in order to analyze the surface morphology of 5SmHAp and 10SmHAp coatings. Therefore, a HITACHI S4500 microscope (Hitachi, Ltd., Tokyo, Japan) equipped with energy-dispersive X-ray spectroscopy (EDX) (Ametek EDAX Inc., Mahwah, NJ, USA) attachment operating at 20 kV was used for coatings investigation.

Fourier transform infrared spectroscopy -attenuated total reflection (FTIR-ATR) was used in order to study functional groups present in the obtained coatings. The FTIR spectra were taken in the spectral range of 400 to 4000 cm^{-1} with a resolution of 4 cm^{-1} with the aid of a Perkin Elmer SP-100 spectrometer (PerkinElmer, Inc., Waltham, MS, USA).

2.5. Broth Microdilution Assay

The 5SmHAp and 10SmHAp were investigated for their *in vitro* antibacterial activity against two Gram negative (*Escherichia coli* 25922 ATCC, *Pseudomonas aeruginosa* 27853 ATCC) and two Gram positive (*Staphylococcus aureus* 25923 ATCC, *Enterococcus faecalis* 29212 ATCC) and for *in vitro* antifungal activity against *Candida albicans* ATCC 10231. The evaluation of the biological activity of the compounds was performed by broth microdilution method. The microbial suspensions were prepared in sterile PBS (phosphate buffer saline) by suspending four to five colonies from 18–24 h pure cultures grown on solid media. The bacterial suspensions adjusted to the McFarland standard 0.5 were further diluted to 1:100 in Muller Hinton broth (MHB). Ten binary dilutions starting from 10 mg/mL (compound stock solution in DMSO) for each of tested compound and DMSO, were prepared in sterile MHB dispensed in 96-well sterile microplates. Each well of the microplates containing the SmHAp solution was inoculated with the microbial suspensions. For each tested compound, a sterility control that contained only broth and a growth control containing broth and microbial inoculum was prepared. The microplates were incubated at $37\text{ }^\circ\text{C}$ for 16–24 h. The MICs values defined as the lowest concentrations of the compound that

inhibited the microbial growth of the tested microbial strains were determined based on the absorbance values assessed spectrophotometrically at 620 nm. The assay was performed in duplicate.

2.6. Antibiofilm Activity

The effects of the compounds on the microbial biofilms were determined as previously described. Using fresh microbial cultures, suspensions were prepared in MHB to obtain a density of 10^7 CFU/mL which were further used for inoculation of 96-well plates containing ten different concentrations of each compound (starting from 10 mg/mL stock solution in DMSO). Wells containing only broth served as negative control and wells containing broth seeded with microbial suspension were used as positive control. The inoculated microplates were incubated at 37 °C for 24 h. The microbial biofilms were evaluated using the crystal violet assay. After incubation, the liquid microbial cultures were gently discarded and the wells were rinsed three times with PBS (pH 7.2) in order to remove the unattached microbial cells. Then, the biofilms were fixed with 150 µL of methanol for 15 min and stained with 1% CV for 15 min at room temperature. The excess dye was washed with PBS, and 150 µL of acetic acid 33% was added to dissolve the crystal violet. The biofilms were evaluated by measuring the absorbance of colored solutions at OD 492 using a microtiter plate spectrophotometer. The minimum biofilm inhibition inhibitory concentration (MBIC) was defined as the lowest concentrations of the compound that inhibited biofilm formation. The experiments were carried out in duplicate.

2.7. In Vitro Biocompatibility Assessment

In vitro cell response to uncoated Si substrate and SmHAp ($x_{Sm} = 0.05$ and 0.1) coatings were analyzed using HGF-1 gingival fibroblasts cell line (purchased from American Type Culture Collection (ATCC), Cat. No. CRL-2014, Rockville, MD, USA). The cells were cultured in Dulbecco's Modified Eagle Medium (DMEM; Gibco/Invitrogen, Carlsbad, CA, USA) with an addition of 10% fetal bovine serum (FBS; Gibco/Invitrogen, Carlsbad, CA, USA) at 37 °C in a humidified atmosphere with 5% CO₂. After 48 h of cell exposure to sterilized samples, several biocompatibility tests were performed.

The cell viability was measured using the 3-(4,5-dimethylthiazol-2-yl)-2,5-diphenyltetrazolium bromide (MTT) assay which is based on the quantification of NAD(P)H-dependent cellular oxido-reductase enzymes activity in the viable cells. Following each treatment interval, the cells were observed by phase contrast microscopy on an inverted Olympus IX71 microscope (Olympus, Tokyo, Japan) to establish the morphological changes and were subsequently incubated with 1 mg/mL MTT solution for 3 h at 37 °C. The medium was then removed and 200 µL of isopropyl alcohol were added to each well to dissolve the produced formazan crystals. The purple formazan crystals formed in the viable cells were dissolved with 2-propanol and the absorbance was measured at 595 nm using a GENiosTecan microplate reader (GENiosTecan, Salzburg, Austria).

The lactate dehydrogenase (LDH) amount released in culture medium was determined as a measure of cell membrane integrity and cell viability using a commercial kit (Cytotoxicity Detection Kit-LDH, Roche, Basel, Switzerland) by reading the absorbance at 490 nm using a microplate reader (GENiosTecan, Salzburg, Austria).

The level of nitric oxide (NO) released in the culture medium as an indicator of inflammation was assessed using the Griess reagent (a stoichiometric solution (*v/v*) of 0.1% naphthylethylenediamine dihydrochloride and 1% sulphanilamide in 5% H₃PO₄) after reading the absorbance at 550 nm.

The cell cytoskeleton morphology was visualized via fluorescence imaging using cells fixed with 4% paraformaldehyde for 20 min and permeabilized with 0.1% Triton X-100—2% bovine serum albumin for 1 h. Filamentous actin (F-actin) was labeled with 20 µg/mL phalloidin conjugated with fluorescein isothiocyanate (FITC) (Sigma-Aldrich, Munich, Germany) and nuclei were counterstained with 2 µg/mL 4',6-diamidino-2-phenylindole

(DAPI) (Molecular Probes, Life Technologies, Carlsbad, CA, USA). Images were captured using a fluorescence microscope Olympus IX71 (Olympus, Tokyo, Japan).

2.8. Statistical Analysis

All data were expressed as mean value \pm SD of three independent experiments. Statistical differences between samples and control were evaluated by Student's *t*-test (Microsoft Excel) and a value of $p < 0.05$ was considered statistically significant.

3. Results

3.1. Samarium Doped Hydroxyapatite Coatings Characterization

In agreement with the XRD patterns (Figure 1), it was revealed that the crystallization of SmHAp samples was slightly influenced by the concentration of Sm. The XRD pattern was presented at angles between $20^\circ < 2\theta < 80^\circ$. The noticed positions of diffraction lines (2θ and corresponding $d_{2\theta}$) were in good agreement with the corresponding values for pure hexagonal HAp (JCPDS, Card No. 9-432) that were previously reported [26]. The peaks at 2θ values were attributed to the pure hexagonal hydroxyapatite structure. The *hkl* values of pure hexagonal HAp peaks are associated to the 002, 102, 210, 211, 112, 300, and 202, respectively [27]. The additional lines of impurities were not observed at the intensity scale established in Figure 1.

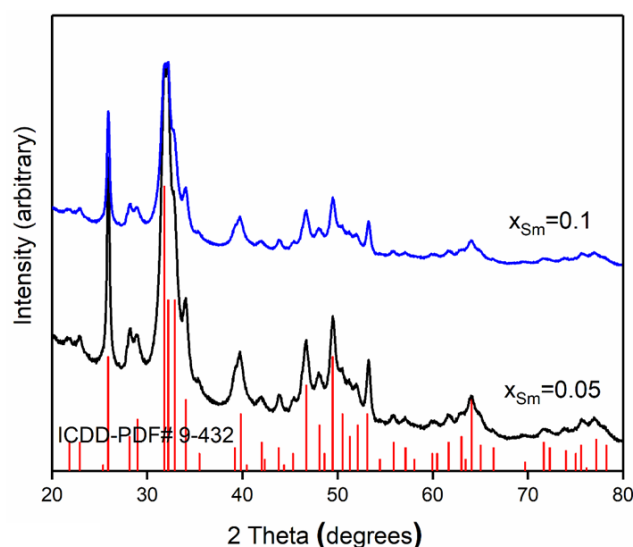


Figure 1. X-ray diffraction pattern of 5SmHAp ($x_{Sm} = 0.05$) and 10SmHAp ($x_{Sm} = 0.1$) in the 2θ range from 20° to 80° .

The functional groups presented in the obtained 5SmHAp and 10SmHAp coatings were investigated by FTIR measurements. The results of the FTIR studies are presented in Figure 2. Thus, both in the case of 5SmHAp and in the case of 10SmHAp coatings could be noticed the presence of main vibrational bands characteristic of the PO_4^{3-} and OH^- groups from the hydroxyapatite (HAp) structure. Also, could be noticed the presence of the vibrational bands specific to adsorbed water. The main vibrational bands presented in the $1600\text{--}1700\text{ cm}^{-1}$ and $3200\text{--}3600\text{ cm}^{-1}$ spectral regions are attributed to O–H bending mode of lattice water [22]. The vibrational band at around 962 cm^{-1} is also specific to phosphate group (ν_1). The main vibrational bands presented at about 1043 and 1091 cm^{-1} are specific to phosphate group (ν_3) [25]. Also, the vibrational bands at around 602 and 566 cm^{-1} are characteristic to ν_4 vibration mode of PO_4^{3-} group from the hydroxyapatite structure. Previous studies [28] have shown that the vibrational bands specific to hydroxyl groups from HAp structure presented at around 632 cm^{-1} and 3568 cm^{-1} could indicate a well crystallized HAp structure. Also, in the Figure 2 it can be seen that the intensity of the vibration bands is decreasing with the increase of the samarium concentration in the

samples. Similar behavior has been reported by D. Predoi et al. in their previous studies conducted on zinc doped hydroxyapatite [29]. Also, in the case of 10SmHAp coatings a slight displacement of the position of the vibrational bands was noticed.

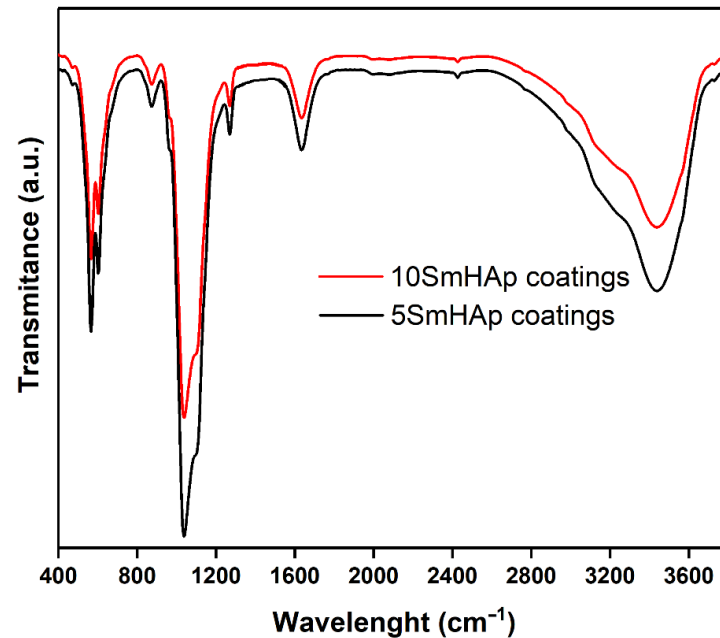


Figure 2. FTIR spectra of 5SmHAp and 10SmHAp coatings deposited on Si substrate.

The surface morphology and chemical composition of 5SmHAp and 10SmHAp coatings were analysed by SEM. The results are shown in Figure 3 (for 5SmHAp coatings) and Figure 4 (for 10SmHAp coatings). The obtained SEM micrographs on the 5SmHAp samples revealed that the coatings surface has a granular structure. Furthermore, the presence of the main chemical elements (samarium, calcium, phosphorus and oxygen) from the structure of samarium doped hydroxyapatite ($x_{Sm} = 0.05$) is highlighted by the EDX spectra (Figure 3 right).

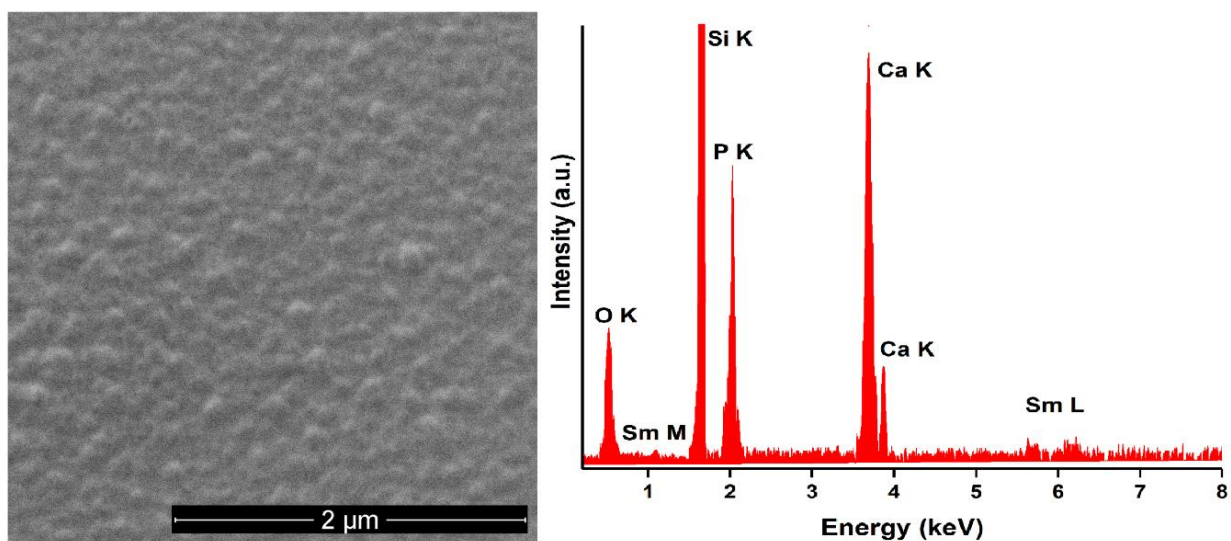


Figure 3. SEM micrograph (left) and EDX spectra (right) obtained on 5SmHAp deposited in Si substrate.

In the Figure 4 (left) could be noticed that the 10SmHAp coatings has a similar granular structure with the one obtained in the case 5SmHAp coatings. Moreover, it can be seen that the granular structure becomes more pronounced with increasing of Sm concentration

in the samples, this behavior being most likely due to the tendency of agglomeration of nanoparticles [25]. Also, the EDX spectra obtained on 10SmHAp confirm the presence of the main chemical elements (samarium, calcium, phosphorus and oxygen). Moreover, in the case of both samples could be noticed that the coatings present no cracks or other discontinuities. In both cases the maximum of Si in the EDX spectra is due to the substrate on which the coatings were deposited. The obtained EDX spectra also revealed and highlighted the coatings purity by the absence of the impurities in the obtained spectra.

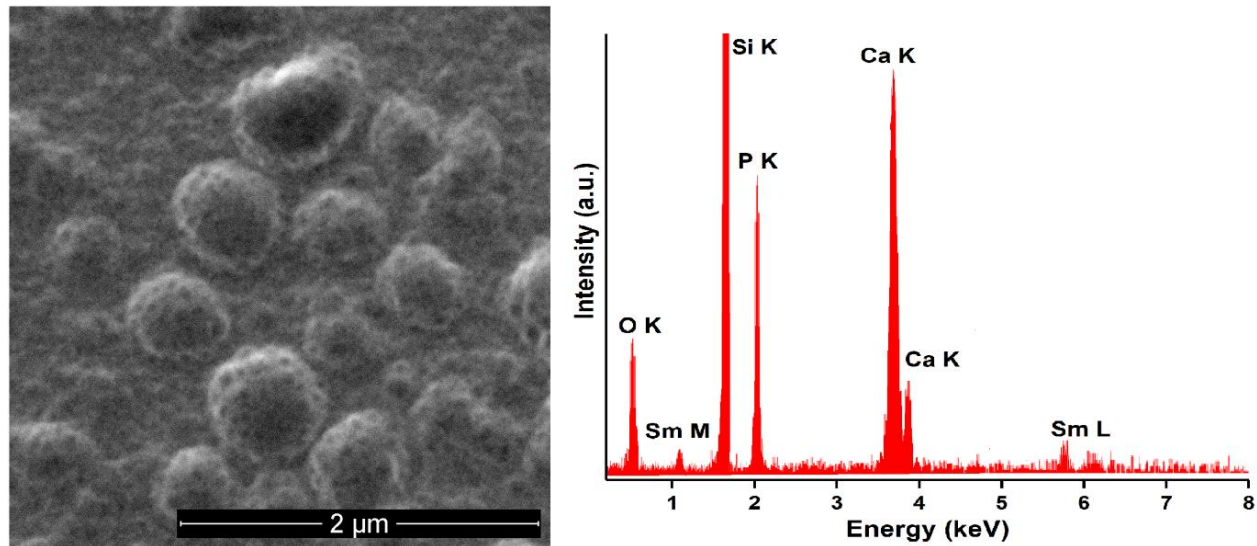


Figure 4. SEM micrograph (left) and EDX spectra (right) obtained on 10SmHAp deposited in Si substrate.

3.2. Antimicrobial Activity

The SmHAp coatings did not exhibit antimicrobial activity at concentration of 5 mg/mL against the tested Gram-positive (*Staphylococcus aureus* 25923 ATCC, *Enterococcus faecalis* 29212 ATCC) and Gram-negative bacteria (*Escherichia coli* 25922 ATCC, *Pseudomonas aeruginosa* 27853 ATCC) and fungal strain (*Candida albicans* ATCC 10231). The effects of the tested compounds on the bacterial attachment and biofilm formation are given in Figures 5 and 6. In comparison to the results obtained on planktonic microbial cells, generally, the compounds exhibited a better antibiofilm activity as demonstrated by the lower MBIC values (1.25 mg/mL), except *P. aeruginosa* biofilm formation which was inhibited by the presence of 5 mg/mL of both compounds. The findings in the present study are indicating that the investigated compounds may hold promise in the development of novel antibiofilm agents.

3.3. Biocompatibility of SmHAp Coatings

The influence of uncoated Si substrates and different coatings containing samarium doped hydroxyapatite on cellular viability and membrane integrity as well as their potential to generate an inflammatory response was evaluated by several *in vitro* tests performed on normal human gingival fibroblasts.

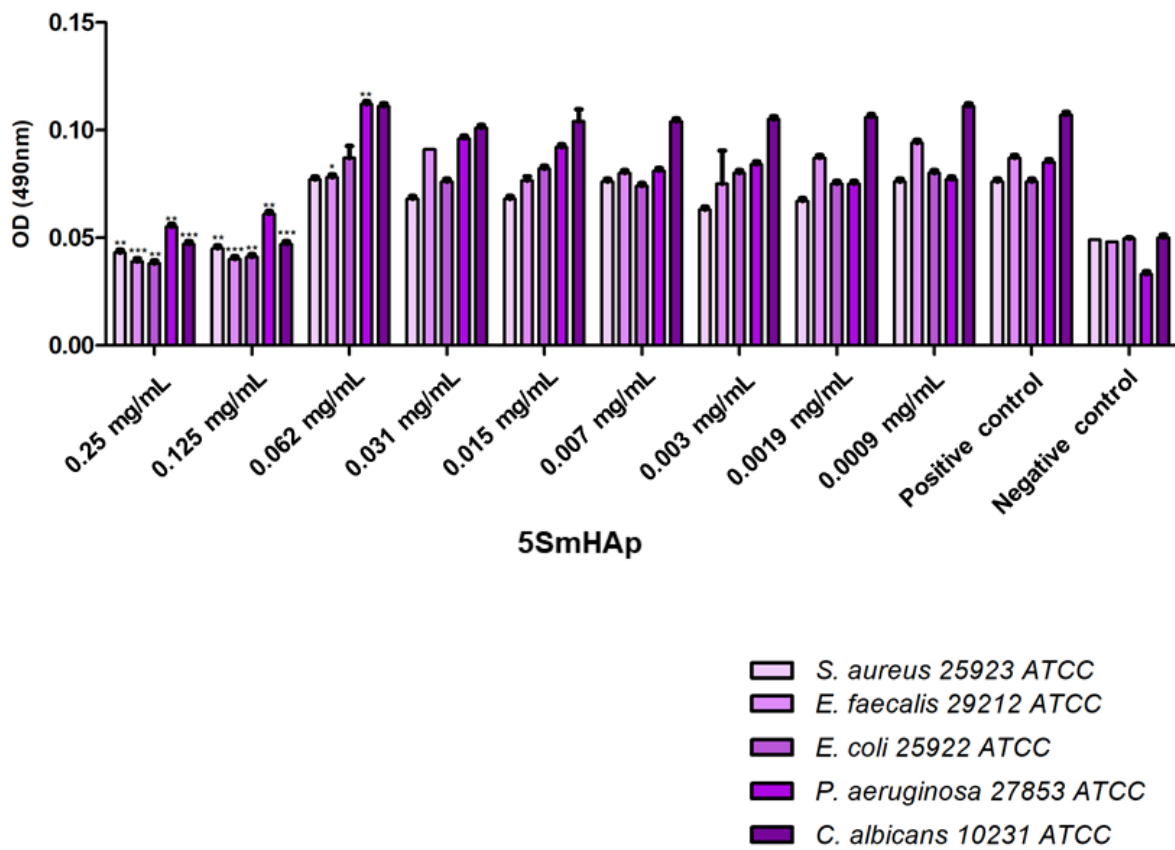


Figure 5. Graphic representation of the antibiofilm activity of 5SmHAp. * $p < 0.05$, ** $p < 0.01$ and *** $p < 0.001$ compared to control.

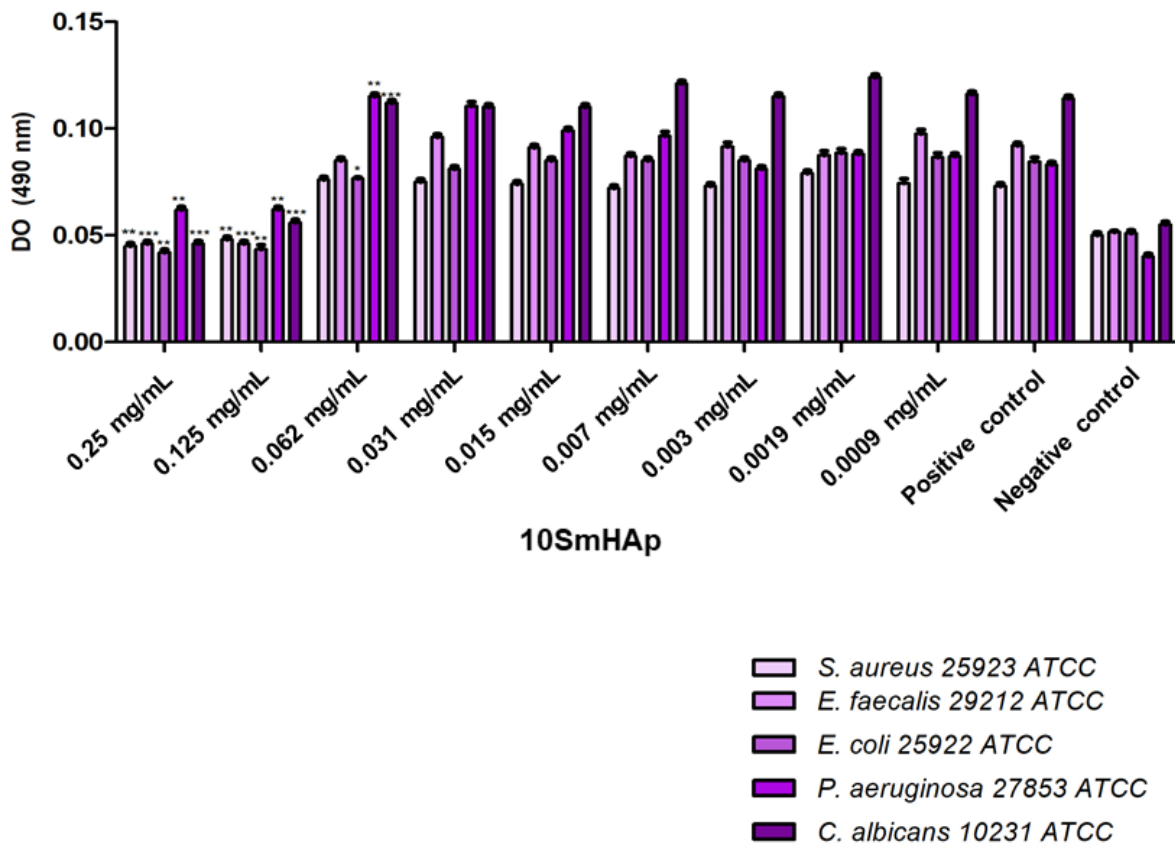


Figure 6. Graphic representation of the antibiofilm activity of 10SmHAp. * $p < 0.05$, ** $p < 0.01$ and *** $p < 0.001$ compared to control.

As shown in Figure 7, after 24 h of exposure to these coatings, no significant changes in gingival cells' viability were recorded. Although very small differences were observed between the uncoated and the treated surfaces, the best biocompatibility was registered for the surfaces coated with samarium doped hydroxyapatite ($x_{Sm} = 0.1$). After 24 h of incubation, the level of intracellular lactate dehydrogenase (LDH) released into the culture medium was close to the control, demonstrating that none of the tested surfaces significantly affected the cell membrane integrity.

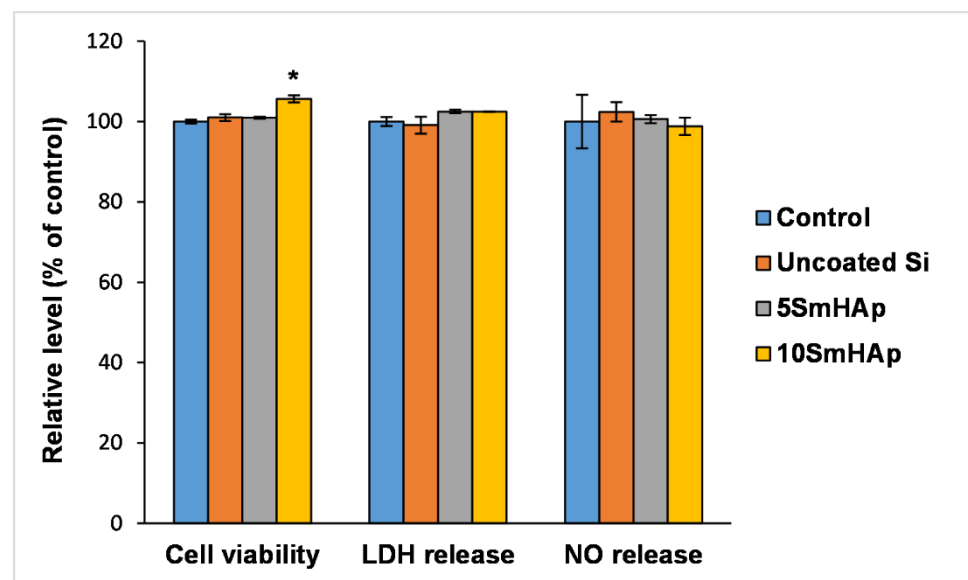


Figure 7. Biocompatibility of uncoated Si substrates and different samarium doped hydroxyapatite coatings as shown by cell viability, lactate dehydrogenase (LDH), and nitric oxide (NO) release assays after 24 h exposure on normal gingival fibroblasts. Results are expressed as the mean \pm standard deviation (SD) ($n = 3$) and represented relative to the untreated cells (control). * $p < 0.05$ compared to control.

For this study, nitric oxide (NO) measurement was used both as a marker of inflammation and as a key regulator of apoptotic death and cellular viability. It is well known that the influence of NO on cell viability is dependent on concentration and cell type; higher levels induce apoptotic death, while lower or moderate concentrations protect the cells, favoring their survival [30]. In the present study, the NO levels released into the culture medium by gingival fibroblasts grown on the both concentration of samarium doped hydroxyapatite coated samples were very close to the control value and the uncoated Si surface.

In addition, for a more complex characterization of the biological response induced in gingival fibroblasts by exposure to these modified Si surfaces with antibiofilm potential, the dynamic changes of the actin cytoskeleton were evaluated. Our results evidenced by the fluorescence microscopy in Figure 8 were consistent with the results of the biocompatibility tests shown in Figure 7. Thus, it was observed that the human cells maintained their specific elongated morphology and established numerous focal adhesions after 24 h of incubation, which confirmed that SmHAp coatings did not affect the behavior of gingival fibroblasts and their proliferative capacity was not disturbed in the presence of the samples, especially in the case of the surface with a higher content of samarium ($x_{Sm} = 0.1$). These modified surfaces were harmless to the gingival cells, proving a good biocompatibility. Moreover, the microscopy images showed that even if cell viability has not changed, several cell-cell fusions have occurred on the surface covered with 5SmHAp, leading to formation of fibroblast-derived multinucleated giant cells as a biomaterial-induced foreign body response.

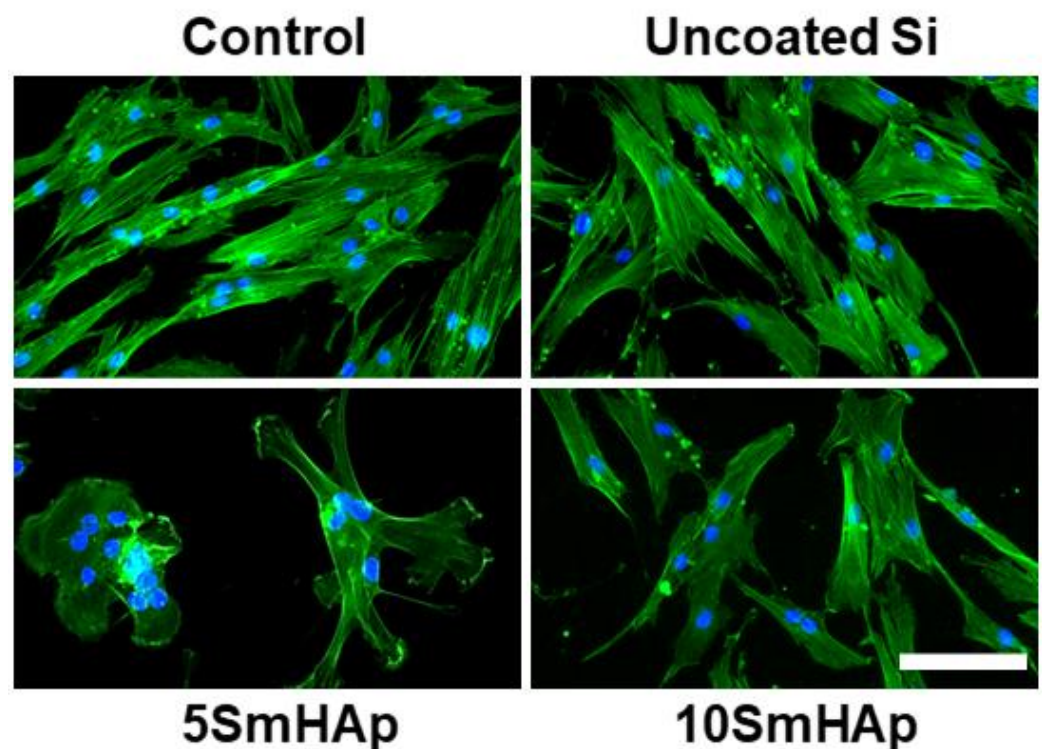


Figure 8. Actin cytoskeleton organization of gingival fibroblast cells after 24 h of incubation with uncoated Si substrates and different samarium doped hydroxyapatite coatings. F-actin (green) was labeled with phalloidin-phalloidin-fluorescein isothiocyanate (FITC) and nuclei (blue) were counterstained with 4',6-diamidino-2-phenylindole dihydrochloride (DAPI). Scale bar: 20 μm .

4. Discussion

The samarium doped hydroxyapatite coatings tested in the present study exhibited good biocompatibility with the gingival cells, as evidenced by F-actin cytoskeleton organization and higher cell proliferation. Similar to the antimicrobial effects, the improved fibroblasts behavior was dependent on the amount of Sm in the coatings, being particularly evident in the sample with a higher Sm content.

Although research on the materials and techniques used in the field of bioimplants has expanded greatly in recent years, there is still a lot of work involved in the development of better biomaterials with functionalized surfaces in order to improve the long-term treatment outcomes. Several approaches such as surface roughness modification and biomolecule immobilization are currently used, but nanotechnology-based biomimetic surfaces are being investigated as a future trend to enhance tissue-implant interaction and thus, improving protein adsorption, cell attachment and mineralization for accelerating the bone healing process [31].

Calcium phosphates are among the most widely used agents for producing bioactive coatings. Because of their higher surface energy, HAp nanoparticles show excellent mechanical properties and resorbability compared to the bulk compound [32]. Different methods are available for the deposition of HAp [$\text{Ca}_{10}(\text{PO}_4)_6(\text{OH})_2$] on metallic implants including thermal spraying, plasma spraying, sol-gel, electrochemical deposition, radio frequency magnetron sputtering, chemical vapor deposition, micro-arc oxidation (MAO), high-velocity suspension flame spraying (HVSFS), or pulsed laser deposition (PLD) [33]. In spite of the fact that thermal spray coating is the most commonly applied nowadays, in this study we showed that efficient and uniform HAp layers can be also obtained on the metal surfaces by dip coating. The obtained results highlighted the fact that by dip coating can be obtained coatings without cracks or other discontinuities and with a granular structure.

Polymicrobial biofilm-associated infections are a primary reason for orthopedic or dental implants failure. The multilayered bacterial cell proliferation in an extracellular polysaccharide matrix always leads to an exacerbated inflammatory response and significant damage of surrounding tissues, resulting in loss of supporting structures [34]. Therefore, alternative strategies aiming to reduce microbial adhesion and control biofilm formation on implanted devices are urgently needed. Doping with rare-earth elements such as Sm^{3+} could increase the antimicrobial properties of HAp-based bioactive coatings. Our findings are in accordance with other results already reported in the literature, proving a direct correspondence between the increase in the amount of metal dopant and antibacterial activity [35]. For this reason, 10SmHAp surfaces were shown to possess a greater potential to inhibit biofilm formation *in vitro*, without affecting the attachment and growth of human gingival fibroblasts, suggesting that these coatings hold promise for developing novel medical devices with antibiofilm properties.

Another factor that has been recognized as critical for the efficiency of the metal implants is their biocompatibility. Successful long-term applications of biomaterials in the medical field are determined not only by physicochemical parameters (composition, surface characteristics, biomechanical factors, implant width, length and geometry) but also by the cytotoxicity of these materials, their compatibility with the host bone and their ability to promote osseointegration of a possible implant without generating severe inflammatory processes in surrounding soft tissues. Multinucleated giant cells formed as a result of cell-cell fusion constitute an integral component of various physiological processes including the biomaterial-induced foreign body response (FBR) [36,37]. Several studies have reported that biomaterials topography can modulate the fusogenic capacity of different cell types [38–40]. In our research, we observed that the granular structure of the tested surface became more pronounced with increasing of Sm concentration and this behavior was correlated with cytoskeletal remodeling in 5SmHAp samples. These results are in good agreement with another study regarding nanotopography-induced cell fusion. Briefly, it showed that cells on flat bulk metallic glass (BMG) were found to be significantly larger and elongated compared to cells on BMG displaying 55 nm nanorods [41]. Also, the discrepancy between the biocompatibility results shown in Figure 7 and the organization of the actin cytoskeleton illustrated in Figure 8 can be explained by the fact that cell viability was measured based on mitochondrial activity that does not change with cell morphology. As shown in Figure 7, the number of viable cells is approximately similar for both surfaces (5SmHAp and 10SmHAp), but lower samarium concentration induced a more pronounced FBR, favoring the formation of fibroblast-derived multinucleated giant cells. Thus, the incorporation of Sm in the HAp nanoparticles endowed the resulting coating with an enhanced cell response and antibiofilm activity, these two key features contributing to a better outcome after bone graft implantation.

5. Conclusions

In the present work, we revealed the obtaining of homogenous and uniform SmHAp coatings with no cracks or fissures using the dip coating method. The results of XRD studies highlighted the slight influence of Sm concentration on the coatings crystallinity. Also, the presence of main vibrational bands associated with the hydroxyl and phosphate group from hydroxyapatite structure were highlighted by FTIR results. The presence of lanthanides (samarium) in the studied samples was confirmed by EDX analysis. Our results highlighted the biocompatibility on human gingival cells of these modified surfaces with enhanced antibiofilm activities. One major limitation of our study are the *in vitro* static experimental conditions. In fact, metal implants are in continuous contact with body fluids (plasma and saliva) and the biofilm formation on biomaterial surfaces is influenced by the multiple pathogen species, host immune cells and the pellicle which rapidly covers a newly implanted device. But if such antibacterial surfaces with sustained *in vitro* efficacy can also withstand the *in vivo* mechanical, chemical, and immunological assaults generated by an infected implant, it will be possible to design new generation biomaterials that will be able

to prevent peri-implantitis and other implant-associated infections in order to reduce bone loss and implant failures.

Author Contributions: Conceptualization, A.D. and D.P.; Data curation, I.C.N., M.P., L.M. and S.C.C.; Formal analysis, I.C.N., S.L.I., S.C.C.; Investigation, I.C.N., M.P., S.L.I. and S.C.C.; Methodology, I.C.N., M.P., S.L.I. and S.C.C.; Project administration, S.C.C. and D.P.; Resources, D.P.; Software, S.L.I.; Supervision, A.D. and D.P.; Validation, L.M. and S.L.I.; Visualization, I.C.N. and S.C.C.; Writing—original draft, I.C.N.; Writing—review & editing, L.M., A.D. and D.P. All authors have read and agreed to the published version of the manuscript.

Funding: This work was supported by the Romanian Ministry of Research and Innovation through the project PN-III-P2-2.1-PED-2019-0868 contract no. 467PED/2020.

Institutional Review Board Statement: Not applicable.

Informed Consent Statement: Not applicable.

Data Availability Statement: Data is available on request from the corresponding author.

Conflicts of Interest: The authors declare no conflict of interest.

References

1. Salehi, G.; Behnamghader, A.; Mozafari, M. Cellular response to metal implants. In *Woodhead Publishing Series in Biomaterials, Handbook of Biomaterials Biocompatibility*, 1st ed.; Mozafari, M., Ed.; Woodhead Publishing: Sawston, UK, 2020; pp. 453–471.
2. Beig, B.; Liaqat, U.; Khan Niazi, M.F.; Douna, I.; Zahoor, M.; Khan Niazi, M.B. Current challenges and innovative developments in hydroxyapatite-based coatings on metallic materials for bone implantation: A review. *Coatings* **2020**, *10*, 1249. [[CrossRef](#)]
3. Gaviria, L.; Salcido, J.P.; Guda, T.; Ong, J.L. Current trends in dental implants. *J. Korean Assoc. Oral Maxillofac. Surg.* **2014**, *40*, 50–60. [[CrossRef](#)] [[PubMed](#)]
4. Müller, V.; Pagnier, T.; Tadier, S.; Gremillard, L.; Jobbagy, M.; Djurado, E. Design of advanced one-step hydroxyapatite coatings for biomedical applications using the electrostatic spray deposition. *Appl. Surf. Sci.* **2020**, *541*, 148462. [[CrossRef](#)]
5. Gadow, N.; Killinger, A.; Stiegler, N. Hydroxyapatite coatings for biomedical applications deposited by different thermal spray techniques. *Surf. Coat. Technol.* **2020**, *205*, 1157–1164. [[CrossRef](#)]
6. López-Valverde, N.; Macedo-de-Sousa, B.; López-Valverde, A.; Ramírez, J.M. Effectiveness of antibacterial surfaces in osseointegration of titanium dental implants: A systematic review. *Antibiotics* **2021**, *10*, 360. [[CrossRef](#)]
7. Ribeiro, M.; Monteiro, F.J.; Ferraz, M.P. Infection of orthopedic implants with emphasis on bacterial adhesion process and techniques used in studying bacterial-material interactions. *Biomater* **2012**, *2*, 176–194. [[CrossRef](#)]
8. Khatoun, Z.; McTiernan, C.D.; Suuronen, E.J.; Mah, T.F.; Alarcon, E.I. Bacterial biofilm formation on implantable devices and approaches to its treatment and prevention. *Heliyon* **2018**, *4*, e01067. [[CrossRef](#)]
9. Souza, J.G.S.; Bertolini, M.M.; Costa, R.C.; Nagay, B.E.; Dongari-Bagtzoglou, A.; Barão, V.A.R. Targeting implant-associated infections: Titanium surface loaded with antimicrobial. *iScience* **2020**, *24*, 102008. [[CrossRef](#)]
10. Hickok, N.J.; Shapiro, I.M.; Chen, A.F. The impact of incorporating antimicrobials into implant surfaces. *J. Dent. Res.* **2018**, *97*, 14–22. [[CrossRef](#)]
11. Grischke, J.; Eberhard, J.; Stiesch, M. Antimicrobial dental implant functionalization strategies -A systematic review. *Dent. Mater. J.* **2016**, *35*, 545–558. [[CrossRef](#)]
12. Wang, Y.; Zheng, K.; Song, S.; Fan, D.; Zhang, H.; Liu, X. Remote manipulation of upconversion luminescence. *Chem. Soc. Rev.* **2018**, *47*, 6473–6485. [[CrossRef](#)]
13. Teo, R.D.; Termini, J.; Gray, H.B. Lanthanides: Applications in cancer diagnosis and therapy. *J. Med. Chem.* **2016**, *59*, 6012–6024. [[CrossRef](#)] [[PubMed](#)]
14. Bao, G.; Wen, S.; Lin, G.; Yuan, J.; Lin, J.; Wong, K.L.; Bünzli, J.C.G.; Jin, D. Learning from lanthanide complexes: The development of dye-lanthanide nanoparticles and their biomedical applications. *Coord. Chem. Rev.* **2021**, *429*, 213642. [[CrossRef](#)]
15. Colman, R.; Alexander, B. The effect of lanthanides and actinides on blood coagulation I Evidence for and properties of a new serum thromboplastin factor. *J. Clin. Investig.* **1964**, *43*, 705–719. [[CrossRef](#)] [[PubMed](#)]
16. Kostova, I.; Manolov, I.; Nicolova, I.; Konstantinov, S.; Karaivanova, M. New lanthanide complexes of 4-methyl-7-hydroxycoumarin and their pharmacological activity. *Eur. J. Med. Chem.* **2001**, *36*, 339–347. [[CrossRef](#)]
17. Dahle, J.T.; Arai, Y. Environmental geochemistry of cerium: Applications and toxicology of cerium oxide nanoparticles. *Int. J. Environ. Res. Public Health* **2015**, *12*, 1253. [[CrossRef](#)]
18. Fricker, S.P. The therapeutic application of lanthanides. *Chem. Soc. Rev.* **2006**, *35*, 524–533. [[CrossRef](#)]
19. Cota, I.; Marturano, V.; Tylkowski, B. Ln complexes as double faced agents: Study of antibacterial and antifungal activity. *Coord. Chem. Rev.* **2019**, *396*, 49–71. [[CrossRef](#)]
20. Panchal, P.K.; Parekh, H.M.; Pansuriya, P.B.; Patel, M.N. Bactericidal activity of different oxovanadium(IV) complexes with Schiff bases and application of chelation theory. *J. Enzyme Inhib. Med. Chem.* **2006**, *21*, 203–209. [[CrossRef](#)]

21. Anderson, P.M.; Wiseman, G.A.; Dispenzieri, A.; Arndt, C.A.; Hartmann, L.C.; Smithson, W.A.; Mullan, B.P.; Bruland, O.S. High-dose samarium-153 ethylene diamine tetramethylene phosphonate: Low toxicity of skeletal irradiation in patients with osteosarcoma and bone metastases. *J. Clin. Oncol.* **2002**, *20*, 189–196. [[CrossRef](#)]
22. Herath, H.M.; Di Silvio, L.; Evans, J.R. In vitro evaluation of samarium (III) oxide as a bone substituting material. *J. Biomed. Mater. Res. A* **2010**, *94*, 130–136. [[CrossRef](#)] [[PubMed](#)]
23. Ciobanu, C.S.; Iconaru, S.L.; Popa, C.L.; Motelica-Heino, M.; Predoi, D. Evaluation of samarium doped hydroxyapatite, ceramics for medical application: Antimicrobial activity. *J. Nanomater.* **2015**, *2015*, 14. [[CrossRef](#)]
24. Iconaru, S.L.; Groza, A.; Gaiaschi, S.; Rokosz, K.; Raaen, S.; Ciobanu, S.C.; Chapon, P.; Predoi, D. Antimicrobial properties of samarium doped hydroxyapatite suspensions and coatings. *Coatings* **2020**, *10*, 1124. [[CrossRef](#)]
25. Ciobanu, S.C.; Iconaru, S.L.; Predoi, D.; Prodan, A.M.; Predoi, M.V. Physico-chemical properties and in vitro antifungal evaluation of samarium doped hydroxyapatite coatings. *Coatings* **2020**, *10*, 827. [[CrossRef](#)]
26. Powder Diffraction File: Inorganic Phases, Joint Committee on Powder Diffraction Standards, Swarthmore (1986) Card No. 9-432. Available online: <https://www.icdd.com/pdfsearch/> (accessed on 10 July 2021).
27. Esmailkhanian, A.; Sharifianjazi, F.; Abouchenari, A.; Rouhani, A.; Parvin, N.; Irani, M. Synthesis and characterization of natural nano-hydroxyapatite derived from turkey femur-bone waste. *Appl. Biochem. Biotechnol.* **2019**, *189*, 919–932. [[CrossRef](#)]
28. Iconaru, S.L.; Motelica-Heino, M.; Predoi, D. Study on europium-doped hydroxyapatite nanoparticles by fourier transform infrared spectroscopy and their antimicrobial properties. *J. Spectrosc.* **2013**, *2013*, 284285. [[CrossRef](#)]
29. Predoi, D.; Iconaru, S.L.; Deniaud, A.; Chevallet, M.; Michaud-Soret, I.; Buton, N.; Prodan, A.M. Textural, structural and biological evaluation of hydroxyapatite doped with zinc at low concentrations. *Materials* **2017**, *10*, 229. [[CrossRef](#)]
30. Bosca, L.; Zeini, M.; Traves, P.G.; Hortelano, S. Nitric oxide and cell viability in inflammatory cells: A role for NO in macrophage function and fate. *Toxicology* **2005**, *208*, 249–258. [[CrossRef](#)]
31. Wang, Q.; Zhou, P.; Liu, S.; Attarilar, S.; Ma, R.L.; Zhong, Y.; Wang, L. Multi-scale surface treatments of titanium implants for rapid osseointegration: A review. *Nanomaterials* **2020**, *10*, 1244. [[CrossRef](#)] [[PubMed](#)]
32. Lu, M.; Chen, H.; Yuan, B.; Zhou, Y.; Min, L.; Xiao, Z.; Zhu, X.; Tu, C.; Zhang, X. Electrochemical deposition of nanostructured hydroxyapatite coating on titanium with enhanced early stage osteogenic activity and osseointegration. *Int. J. Nanomed.* **2020**, *15*, 6605. [[CrossRef](#)] [[PubMed](#)]
33. Surmenev, R.A.; Surmeneva, M.A. A critical review of decades of research on calcium-phosphate-based coatings: How far are we from their widespread clinical application? *Curr. Opin. Biomed. Eng.* **2019**, *10*, 35–44. [[CrossRef](#)]
34. Nguyen, V.; Hao, J.; Chou, J.; Oshima, M.; Aoki, K.; Kuroda, S.; Kaboosaya, B.; Kasugai, S. Ligature induced peri-implantitis: Tissue destruction and inflammatory progression in a murine model. *Clin. Oral Implant. Res.* **2017**, *28*, 129–136. [[CrossRef](#)] [[PubMed](#)]
35. Khadar, Y.S.; Balamurugan, A.; Devarajan, V.P.; Subramanian, R.; Dinesh Kumar, S. Synthesis, characterization and antibacterial activity of cobalt doped cerium oxide (CeO₂: Co) nanoparticles by using hydrothermal method. *J. Mater. Res. Technol.* **2019**, *8*, 267–274. [[CrossRef](#)]
36. Ogle, B.M.; Cascalho, M.; Platt, J.L. Biological implications of cell fusion. *Nat. Rev. Mol. Cell Biol.* **2005**, *6*, 567–575. [[CrossRef](#)]
37. Zhang, L.; Cao, Z.; Bai, T.; Carr, L.; Ella-Menye, J.R.; Irvin, C.; Ratner, B.D.; Jiang, S. Zwitterionic hydrogels implanted in mice resist the foreign-body reaction. *Nat. Biotechnol.* **2013**, *31*, 553–556. [[CrossRef](#)]
38. Yim, E.K.; Darling, E.M.; Kulangara, K.; Guilak, F.; Leong, K.W. Nanotopography-induced changes in focal adhesions, cytoskeletal organization, and mechanical properties of human mesenchymal stem cells. *Biomaterials* **2010**, *31*, 1299–1306. [[CrossRef](#)]
39. Jeong, H.; Simon, C.G., Jr.; Kim, G. A mini-review: Cell response to microscale, nanoscale, and hierarchical patterning of surface structure. *J. Biomed. Mater. Res. B Appl. Biomater.* **2014**, *102*, 1580–1594. [[CrossRef](#)]
40. Yang, H.S.; Lee, B.; Tsui, J.H.; Macadangdang, J.; Jang, S.Y.; Im, S.G.; Kim, D.H. Electroconductive nanopatterned substrates for enhanced myogenic differentiation and maturation. *Adv. Healthc. Mater.* **2016**, *5*, 137–145. [[CrossRef](#)]
41. Padmanabhan, J.; Augelli, M.J.; Cheung, B.; Kinser, E.R.; Cleary, B.; Kumar, P.; Wang, R.; Sawyer, A.J.; Li, R.; Schwarz, U.D.; et al. Regulation of cell-cell fusion by nanotopography. *Sci. Rep.* **2016**, *6*, 33277. [[CrossRef](#)]